npg

ORIGINAL ARTICLE

Optically controlled elastic microcavities

Assegid Mengistu Flatae[1,2], Matteo Burresi[2,3], Hao Zeng[2], Sara Nocentini[2], Sarah Wiegele[1],
Camilla Parmeggiani[2,3], Heinz Kalt[1] and Diederik Wiersma[2]

Whispering gallery mode (WGM) resonators made from dielectrics like glass or polymers have outstanding optical properties like huge cavity quality (*Q*) factors which can be achieved on scales compatible with on-chip integration. However, tunability of these resonances is typically difficult to achieve or not suitable for robust device applications. We report here on the fabrication of polymeric micro-goblet WGM resonators with an optically controlled and stable reversible tunability over a large spectral range. This tunability is achieved by integration of photo-responsive liquid crystalline elastomers (LCEs) into micro-goblet cavities. The optical response of the elastomer allows reshaping the goblet by employing low pump power, leading to a fully reversible tuning of the modes. The structure can be realistically implemented in on-chip devices, combining the ultra-high *Q* factors, typical of WGM resonators, with reliable, optical tunability. This result serves as an example of how light can control light, by invoking a physical reshaping of the structure. This way of optical tuning creates interesting possibilities for all-optical control in circuits, enabling interaction between signal and control beams and the realization of self-tuning cavities.

INTRODUCTION

Solid-state optical microcavities are versatile photonic devices which come in a large variety of appearances.[1] Of particular interest are whispering gallery mode (WGM) resonators which feature small modal volume and large quality (*Q*) factors.[2] They are highly attractive for fundamental physics studies like cavity quantum electrodynamics,[3] as well as for applications like single photon sources,[4] optical sensing[5] or communication technology.[6,7] A key feature of WGM microcavities is the occurrence of ultra-narrow optical resonances and the functionality of the cavity often relies on the shift of the resonance frequency. This is the case, e.g., for optical sensors where the modal shift indicates the presence of attached bio-molecules or a change in the composition of the surrounding medium.[5] Essential features of such resonators are thus a large free spectral range and a narrow linewidth of the resonances but for many applications additionally an active manipulation of the cavity resonances is required. Examples are the tuning of the cavity into resonance with a quantum emitter[8,9] or utilization of the cavity in optical filters and light modulators.[10]

In the last decade, a new class of WGM resonators has emerged featuring ultra-high *Q* factors. These resonators have spherical, cylindrical, toroidal, disk or goblet shapes[1,9,11] and are made of silica, polymers or liquids. Besides their excellent sensing capabilities they can also be turned into micro-lasers when incorporating laser dyes[12] or quantum dots[13] or be coupled to form photonic molecules.[14] But an obstacle effectively hindering some applications of these cavities is the limited tunability of these cavities. This is different for semiconductor-based WGM cavities where tuning of the cavity resonances is achievable by temperature-, field- or carrier-induced changes of the optical properties.[15–18] Liquid WGM resonators have been tuned by changing the size of the droplet resonators[19] or by mechanical size stretching.[20–22] But functional facility and reversibility are difficult to attain. By utilizing the birefringence and electric-field induced structural deformation of liquid crystals (LCs), researchers also reported shifting of cavity modes using LCs as a cladding layer,[23] LC-droplet resonators[24] or by immersing semiconductor microcavities in LC solution.[25] However, all these methods do not show controllable reversible tunability and are not suitable to be integrated into a single on-chip device at the same time.

In the following, we will introduce a possibility for reversible, dynamic tuning of polymeric WGM resonators. This tunability is based on the photo-induced shape modification of liquid crystalline elastomer (LCE) actuators integrated into goblet resonators.

MATERIALS AND METHODS

Sample fabrication

Our polymeric WGM resonators are lithographically structured Poly(methyl methacrylate) (PMMA) disks on a silicon chip using a subsequent thermal procedure to achieve the goblet-type cavity geometry.[11] These resonators are compatible with large-scale fabrication and are mechanically stable. Tunability of the cavity resonances is linked to the control of the resonator diameter. To this end, a photo-responsive smart material, a nematic LCE containing an azo-dye is integrated into the goblet geometry. LCEs are solid-state materials that

combine orientational order of a liquid crystal with the elastic properties of long, crosslinked polymer chains.

In the first step we fabricated active polymeric WGM lasers. The laser dye Pyrromethene 597 (PM 597) was doped into a PMMA host matrix with a dye concentration of 12 μmol g$^{-1}$ solid PMMA. This laser dye emits in the visible spectrum near 600 nm, has a high molar absorption coefficient ($\sim 10^5$ M^{-1} cm^{-1}) and near unity quantum yield.[26] The doped PMMA (MicroChem PMMA 950k A7 dissolved in anisole) (Micro Resist Technology GmbH, Berlin, Germany) is spin coated on the top of a silicon wafer to result in a 1 μm thick layer. Circular resonator structures are patterned into the PMMA layer using e-beam lithography (with a dose current of 500 pA). Developing the sample and isotropically etching the exposed silicon using XeF$_2$ results in polymeric micro-disk resonators on a silicon pedestals (see Ref. 11 for more information on the fabrication process and the optical properties of PMMA based micro-resonators).

The second constituent of each tunable resonator, namely the photo-responsive nematic LCE micro-cylinders are produced using two-photon absorption induced polymerization of LC mixtures with direct laser writing (DLW). The DLW allows for 3D high spatial resolution and is used for polymerization and crosslinking of all the LC mixtures. The LC monomer mixtures are composed of LC mesogens, crosslinkers (SYNTHON Chemicals GmbH & Co. KG, Wolfen, Germany), photo-initiators (Irgacure 369) (Sigma-Aldrich Chemie GmbH, Munich, Germany) and an azo-dye (European Laboratory for non linear spectroscopy, Florence, Italy). Here the LC mesogens provide good nematic alignment of the molecules and the liquid crystalline properties to the final polymer; the photo-initiator is used to trigger a chain reaction for polymerization under ultraviolet (two-photon) exposure while the crosslinkers are essential to obtain elastomeric properties in the entire polymer structure. The actual composition of the LC is 71% of LC mesogens, 2% of photo-initiator, 26% of crosslinker and about 1% of azo-dye (the compositions are percentage by mass). The chemical structure of the mixture is shown in Figure 1a. This mixture is infiltrated into a cell made from glass plates with 50-μm gap. The glass plates are coated with special polyimide (PI1211 Nissan Chemical Industries) to initiate 90° pretilt angle uniaxial alignments of the LC molecules (perpendicular to the glass substrate). Two photon absorption polymerization of the infiltrated LC monomer mixture was induced by 130 femtosecond focused laser at 780 nm from a commercial DLW work station (Photonic Professional; Nanoscribe GmbH). The LCE micro-cylinder structures were written on the bottom inner surface of the glass plate, and the sample position
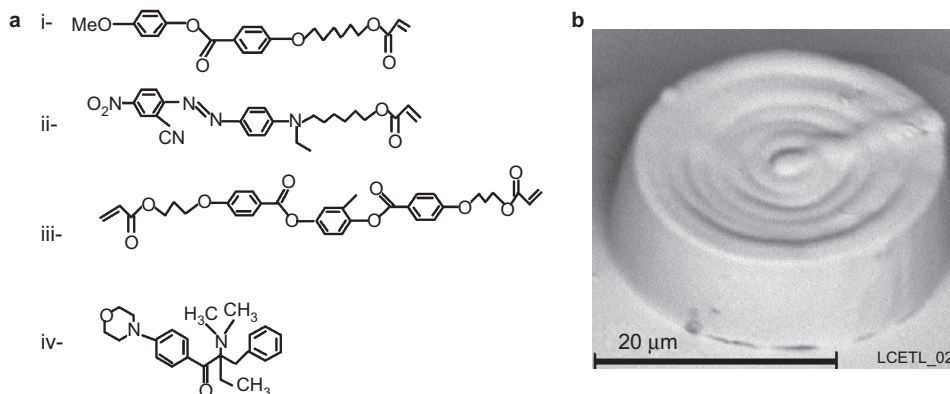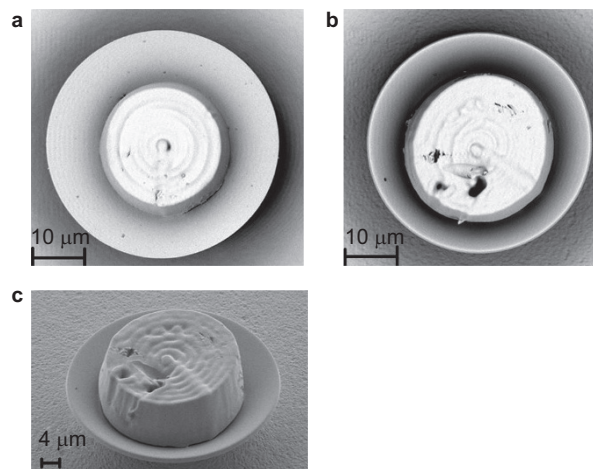
Figure 2 Scanning electron micrograph image. (**a**) LCE/microdisk resonator: a LCE micro-cylinder is centered on-top of a microdisk resonator supported by silicon pedestal. (**b**) The heat reflow process leads to surface-tension induced LCE/microgoblet resonator geometry and fuses the elastomer into the base of the resonator. The dark spots are defects resulting from the micro-tip handling. (**c**) Top-side view of LCE/goblet resonator. LCE, liquid crystalline elastomer.

is controlled by 3D piezo translational stage. DLW followed by developing the sample with toluene leads to LCE micro-cylinder structures, as depicted in Figure 1b. The molecular alignment (director) is along the axis of the cylinder.

The role attributed to the photo-responsive azo-dye is the enhancement of the local temperature of the LCE cylinder (which will be embedded in the goblet resonator) when it undergoes fast trans-cis isomerization *via* the absorption of resonant photons. Commonly commercial azo-dyes have maximum absorption for the photo-isomerization at about 350 nm.[27,28] Hence, these dyes are not suited for DLW polymerization process as this wavelength overlaps with the two photon absorption peak of the photo-initiator. For this reason the absorption maximum of the azo-dye is tuned to around 530 nm by changing the substituent on the aromatic rings.[29] This also coincides with the pump wavelength of PM 597-doped laser cavities.

After fabrication by DLW, the LCE cylinders are centered on top of the PMMA micro-disk resonators using a micro-positioning system. The cylinders can easily be detached from its glass substrate upon heating the sample to 100 ℃ for 10–15 min. We used micro-tips (made from optical fibers) to place the LCE micro-cylinders (25 μm diameter, 10 μm height) on top of polymeric micro-disk resonators

Figure 1 (**a**) Components of the monomer mixture: (i) LC mesogens; (ii) azo-dye; (iii) crosslinker and (iv) photo-initiator. (**b**) Scanning electron micrograph image of a LCE microcylinder polymerized by two-photon absorption 3D DLW. DLW, direct laser writing; LCE, liquid crystalline elastomer; 3D, Three-dimensional; LC, liquid crystals.

(diameter 49 μm) as shown in Figure 2a. The next step is a thermal reflow treatment[11] which leads to the surface-tension induced goblet structure, smoothens the surface of the cavity and fuses the LCE into the base of the goblet resonator. To this end the resonators are placed for 30–40 s on a hot plate at temperature of 125 ℃ (slightly above the glass transition temperature of PMMA). The shape transition reduces the diameter of the cavity to 45 μm. Scanning electron micrograph images of a LCE/goblet resonator are shown in Figure 2b and 2c.

RESULTS AND DISCUSSION

Resonator Q factor

It is important to test whether the optical quality of the goblet resonators is affected by the integration of the LCE micro-cylinders. To measure the Q factor, we used a tapered fiber to evanescently couple visible light (of wavelength around 630 nm) into the LCE/microgoblet resonator. The transmitted light is collected *via* a photo-diode (the experimental set-up is shown in Supplementary Fig. S3). The transmission spectrum (Figure 3) of the fiber recorded with a narrow-band, continuously swept tunable diode laser (632.5–637 nm) reveals the typical WGM structures including fundamental as well as higher order resonator modes. The free spectral range ($\delta\lambda_{FSR}$), which is observed from the periodic repetition of the modal pattern, is 1.95 nm near 635 nm wavelength range. This is in a good agreement with the theoretically expected value of 1.90 nm for a 45 μm diameter PMMA-based micro-goblet. The Q factor is determined from the full width at half maximum of one of the Lorentzian-shaped resonances (see inset of Figure 3). We find a Q factor of about 2.14×10^4 which is in similar order to the Q factor achieved for dye-doped polymeric resonators without LCEs. The Q factor obviously does not deteriorate which is actually no surprise since the WGMs are confined near the rim of the goblet resonator while the LCE is situated at the center.

Tuning of micro-goblet lasing

Illumination of the LCE/PMMA goblet resonators with nanosecond laser pulses in the green spectral range has two consequences. For one, the LCE exhibits a pronounced photo-induced mechanical deformation: the LCE micro-cylinder shows a radial expansion perpendicular to the alignment of the LCE molecules and a simultaneous contraction parallel to the cylinder axis. Second the PM 597 dye-doped polymeric cavity is pumped into laser emission. It is important to note the involved time scales of the experiment: the time scale for the thermal response of the LCE is long compared to the temporal spacing of the

pump pulses nanosecond excitation. The (stimulated) recombination time of the excited laser dye, however, is short compared to the nanosecond pulse duration. Thus, LCE/goblet laser system can be operated under controlled quasi-stationary conditions.

The LCE/PMMA micro-goblet laser cavities were pumped with 10 ns pulses from a frequency-doubled neodymium-doped yttrium orthovanadate (Nd:YVO$_4$) laser at a pump wavelength of 532 nm and a repetition rate of 1 kHz. The pulse duration below 100 ns is essential to prevent triplet formation of the dye molecules, which would inhibit lasing. The excitation pump beam is focused in a free-space micro-photoluminescence (μ-PL) set-up under an angle of 45° to a spot size of about 65 μm diameter to achieve nearly homogeneous excitation of the whole cavity (the laser cavity and the LCE are here pumped by the same laser pulse. This is due to the fact that the azo-dye had to be chemically modified by changing its aromatic ring to shift the absorption wavelength. For realistic applications, it is straightforward to separate the excitation of the laser and the LCE, e.g., by splitting the beam and chose different foci). The emission from the cavity is collected perpendicular to the resonator axis by a microscope objective of NA=0.4 (50×) and directed to a spectrometer (grating with 1200 lines mm^{-1}, of resolution 60 pm) equipped with CCD (charge coupled device) camera. This set-up also provides spatially resolved information about the emitted laser modes along the vertical diameter of the cavity utilizing the dimension of the CCD pixel array parallel to the alignment of the spectrometer entrance slit (the experimental set-up is shown in Supplementary Fig. S4).

The excitation energy density of the pump laser was varied using a Pockels cell along with a linear polarizer. The output emission of the microcavity was then recorded as a function of the pump energy deposited on the cavity per pulse. A characteristic input-output curve of LCE/PMMA micro-goblet dye laser is depicted in Figure 4a. The output intensity at certain pump energy was determined by integrating the intensity of a single lasing mode. The onset of lasing was inferred from the super-linear increase of the intensity resulting from the dominance of stimulated emission over spontaneous emission. The lasing threshold was found to be 0.15 μJ pulse^{-1}. The wavelengths of the laser modes are stable for fixed pump energy since the thermally determined size of the cavity is stationary for a repetition rate of 1 kHz.

For pump energies well above the threshold, several narrow lasing peaks appear in the spectrum (Figure 4b). The spectral distance between adjacent lasing peaks is below the free spectral range of the cavity (about 1.7 nm in the displayed wavelength range). This shows
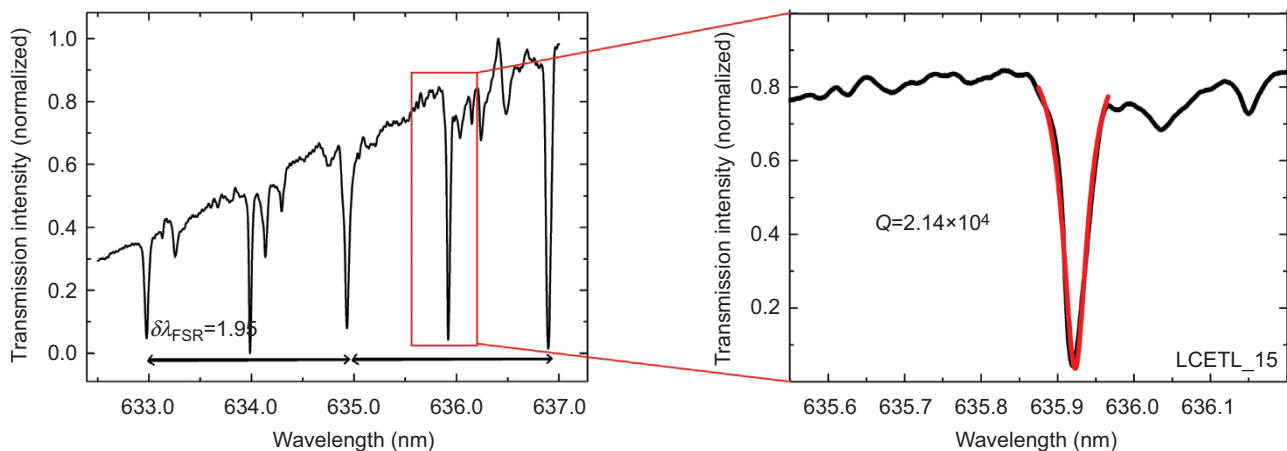
Figure 3 The transmission spectrum of an evanescently coupled tapered fiber shows WGM resonances with a free spectral range of $\delta\lambda_{FSR}$=1.95 nm. LCE/goblet resonators retain a high-Q factor of 2.14×10^4 around 635.9 nm (right inset). LCE, liquid crystalline elastomer; WGM, whispering gallery mode.
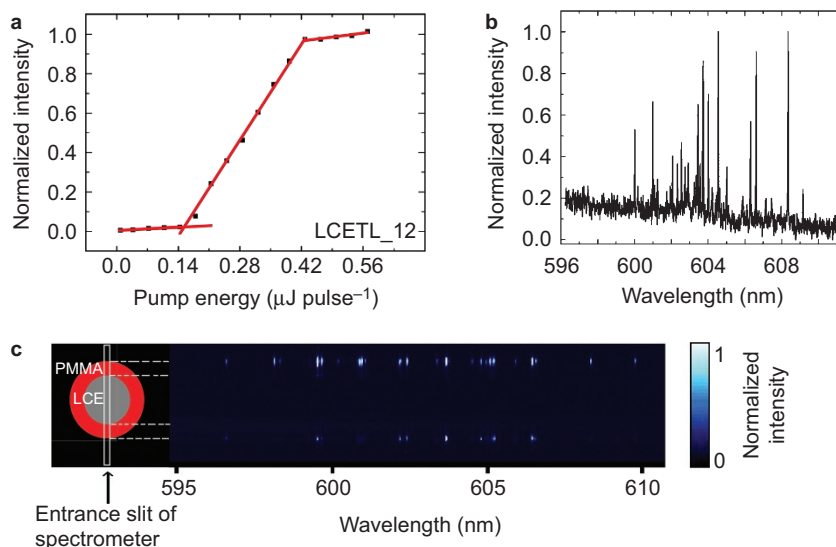
Figure 4 (**a**) Input–output curve of a PM 597 dye-doped LCE/PMMA goblet micro-laser showing a threshold energy of 0.15 µJ pulse^{-1} and a saturation above 0.42 µJ pulse^{-1}. (**b**) WGM laser emission from LCE/goblet resonator at pump energy of 0.28 µJ pulse^{-1} (well above the lasing threshold). (**c**) Image of LCE/goblet WGM lasing mode by the CCD behind the spectrometer, which detects the spectrally resolved PL with a spatial resolution in the vertical direction (white rectangle). The measurement shows that the lasing modes are confined only to the rim of the resonator and the LCE cylinder has no impact on the modal structure of the PMMA goblet resonator. LCE, liquid crystalline elastomer; PL, photoluminescence; PM 597, Pyrromethene 597; WGM, whispering gallery mode; PMMA, Poly(methyl methacrylate).

that besides the fundamental modes, also several higher order cavity modes contribute to the lasing spectrum well above lasing threshold. By aligning the spectrometer entrance slit with the vertical diameter of the sample, as shown in Figure 4c, we also spatially resolved the emitted light along this direction. This measurement confirms that the lasing modes are still confined near the rim of the goblet resonator and that the LCE micro-cylinder does not affect the modal structure of the cavity.

However, the response of the LCE to the optical pumping has significant influence on the spectral position of the cavity resonances. This is demonstrated by recording the modal spectrum for different excitation energies (Figure 5 (left)). We find a pronounced reversible red shift of the lasing modes. The maximum shift is as high as 3.5 nm for the first mode surpassing lasing threshold. In Figure 5, we only

show the modal spectrum around the saturation level of the micro-laser in order to be able to track each individual mode separately without any change in spectrum due to newly emerging modes. The red shift can be attributed to the shape deformation of the LCE micro-cylinder. Since the azo-dye is modified to efficiently absorb photons around 530 nm, the pump laser induces an increase in the local temperature of the elastomer. As a result, the aligned molecular network of the LCE, which has been intentionally aligned along the axis of the cylinder, becomes disordered, evoking an in-plane symmetrical expansion of the micro-cylinder (see illustration in Figure 5 (right)). This in turn leads to a symmetrical expansion of the goblet resonators and thus the red shift of the lasing modes. Imaging of the LCE/PMMA goblet resonator to a CCD camera under low repetition-rate pumping directly shows this
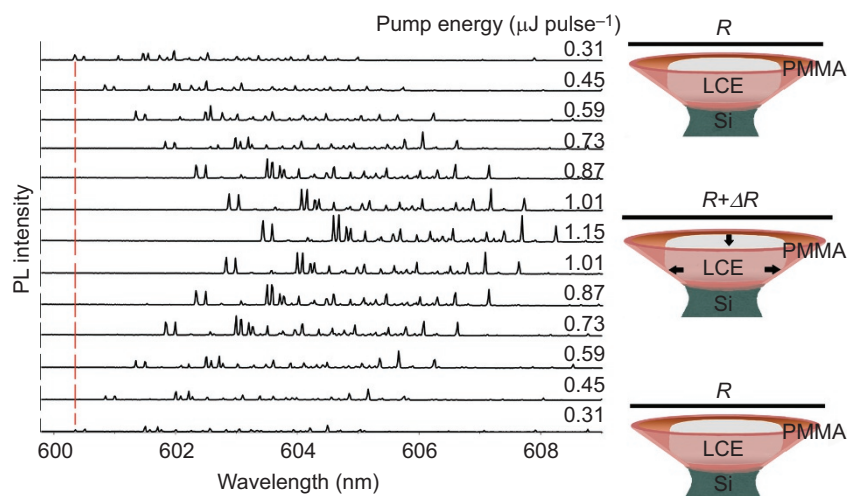
Figure 5 Left: Photo-induced tuning of LCE/goblet laser modes for different pump energies. Increasing the excitation energy from 0.31 µJ pulse^{-1} to 1.15 µJ pulse^{-1} leads to a red shift of the modes of about 3.1 nm. Decreasing the pump power from 1.15 µJ pulse^{-1} back to 0.31 µJ pulse^{-1} results in a reversed spectral shift (blue shift). Right: Schematic diagram of LCE/goblet resonators. Increasing the pump energy increases the disorder in the molecular network of the LCE micro-cylinder and leads to a symmetrical expansion of the LCE structure and the goblet resonator. Decreasing the pump power restores the ordered phase of the elastomer, leading to a perfectly reversible resonator size deformation and tuning of the lasing modes. LCE, liquid crystalline elastomer; PL, photoluminescence.

photo-induced shape modification (Supplementary Movies 1 and 2, and a text file are provided in supplementary information supporting our interpretation).

The photo-induced change in the shape of the LCE/PMMA goblets is found to be linear dependent on pump energy and perfectly reversible. As the pump energy is decreased, the decrease in the temperature of LCE micro-cylinder restores the nematic ordering of the LCE and the goblet shrinks back to its original size. The resulting reversal of the spectral shift is obvious in Figure 5. The lasing modes show red shift of about 0.51 nm for every increase in the excitation energy by 0.14 μJ pulse^{-1}. A decrease in the pump energy by the same amount leads to 100% reversible spectral shift in the first two cycles. The red broken line in Figure 5 shows the perfect reversibility of the first laser mode located at 600.35 nm at pump energy of 0.31 μJ pulse^{-1}. Further measurement in the excitation energy density cycles show the reversibility of the laser modes with fluctuations of the exact modal positions in the 0.1 nm range. Plotting the modal shifts as a function of deposited pump energy (not shown) for one measurement cycle, we find a perfect linear dependence with a slope of 3.64 nm μJ^{-1}. This corresponds to an expansion (contraction) of the radius of the cavity by nearly 27.3 nm for every 0.1 μJ increase (decrease) in input pump energy for the here discussed regime near the saturation level of the micro-laser.

In the following, we demonstrate that the modification of the modal wavelengths of the polymeric cavity is not caused by heating of the cavity itself. In principle heat can cause a shift of the cavity modes due to the negative thermo-optic coefficient of PMMA. Thus, we replaced the LCE micro-cylinders by negative photo-resist (IP–L; Nanoscribe GmbH) micro-cylinders of similar size doped with azo-dye (same concentration as in LCE mixture) and fabricated using 3D laser writing. We find no spectral shift of the cavity modes when pumping in the energy-density range used for the experiments described above. Hence, we can exclude a direct heating of the PMMA cavity and the observed spectral shifts of LCE/goblet resonator modes is solely due to the photo-induced deformation of the LCE.

CONCLUSIONS

In this paper, we present a method for an optically controlled, stable and reversible tuning of whispering gallery modes in polymeric high-*Q* resonators over a large spectral range. To this end, solid-state, nematically ordered LCE micro-cylinders are placed onto dye-doped PMMA micro-disk resonators. A thermal reflow process leads to smooth cavity surfaces, a goblet-type cavity geometry and integrates the LCE within the goblet basis. We prove that this integration technique maintains the modal structure and the high *Q* factor of the resonators. Upon optical pumping, the symmetrical deformation of the LCE micro-cylinders leads to expansion of the polymeric goblet resonators and to a related red shift of the laser modes. Decreasing the pump power yields the reversed spectral shift. The spectral shift is linear in the change of deposited pump energy and reproducible. Although some of the processing steps still have to be optimized, the demonstrated photo-induced tunability of WGM resonators is highly attractive for fundamental studies as well as device applications where tunability is often required.

1   Vahala KJ. Optical microcavities. *Nature* 2003; **424**: 839–846.
2   Armani DK, Kippenberg TJ, Spillane SM, Vahala KJ. Ultra-high-*Q* toroid microcavity on a chip. *Nature* 2003; **421**: 925–928.
3   Khitrova G, Gibbs HM, Kira M, Koch SW, Scherer A. Vacuum Rabi splitting in semiconductors. *Nat Phys* 2006; **2**: 81–90.
4   Michler P, Kiraz A, Becher C, Schoenfeld WV, Petroff PM *et al.* A quantum dot single-photon turnstile device. *Science* 2000; **290**: 2282–2285.
5   Vollmer F, Arnold S. Whispering-gallery-mode biosensing: label-free detection down to single molecules. *Nat Methods* 2008; **5**: 591–596.
6   Djordjev K, Choi SJ, Dapkus PD. Microdisk tunable resonant filters and switches. *IEEE Photonics Technol Lett* 2002; **14**: 828–830.
7   Rabiei P, Steier WH, Zhang C, Dalton LR. Polymer micro-ring filters and modulators. *J. Lightwave Technol* 2002; **20**: 1968–1975.
8   Srinivasan K, Michael CP, Perahia R, Painter O. Investigations of a coherently driven semiconductor optical cavity QED system. *Phys Rev A* 2008; **78**: 033839.
9   Peter E, Senellart P, Martrou D, Lemaitre A, Hours J *et al.* Exciton-photon strong-coupling regime for a single quantum dot embedded in a microcavity. *Phys Rev Lett* 2005; **95**: 067401.
10   Hryniewicz JV, Absil PP, Little BE, Wilson RA, Ho PT. Higher order filters response in coupled microring resonators. *IEEE Photonics Technol Lett* 2000; **12**: 320–322.
11   Grossmann T, Hauser M, Beck T, Gohn-Kreuz C, Karl M *et al.* High-*Q* conical polymeric microcavities. *Appl Phys Lett* 2010; **96**: 013303.
12   Grossmann T, Klinkhammer S, Hauser M, Floess D, Beck T *et al.* Strongly confined, low-threshold laser modes in organic semiconductor microgoblets. *Opt Express* 2011; **19**: 10009–10016.
13   Flatae A, Grossmann T, Beck T, Wiegele S, Kalt H. Strongly confining bare core CdTe quantum dots in polymeric microdisk resonators. *APL Mater* 2014; **2**: 012107.
14   Grossmann T, Wienhold T, Bog U, Beck T, Friedmann C *et al.* Polymeric photonic molecule super-mode lasers on silicon. *Light Sci Appl* 2013; **2**: e82, doi:10.1038/lsa.2013.38.
15   Chang QJ, Li Q, Zhang ZY, Qiu M, Ye T *et al.* A tunable broadband photonic RF phase shifter based on a silicon microring resonator. *IEEE Photonics Technol Lett* 2009; **21**: 60–62.
16   Tapalian HC, Laine JP, Lane PA. Thermooptical switches using coated microsphere resonators. *IEEE Photonics Technol Lett* 2002; **14**: 1118–1120.
17   Wang TJ, Chu CH, Lin CY. Electro-optically tunable microring resonators on lithium niobate. *Opt Lett* 2007; **32**: 2777–2779.
18   Srinivasan K, Painter O. Optical fiber taper coupling and high-resolution wavelength tuning of microdisk resonators at cryogenic temperatures. *Appl Phys Lett* 2007; **90**: 031114.
19   Tang SKY, Derda R, Quan Q, Lončar M, Whitesides GM. Continuously tunable microdroplet-laser in microfluidic channel. *Opt Express* 2011; **19**: 2204–2215.
20   Saito M, Shimatani H, Naruhashi H. Tunable whispering gallery mode emission from a microdroplet in elastomer. *Opt Express* 2008; **16**: 11915–11919.
21   Ta VD, Chen R, Sun HD. Tuning whispering gallery mode lasing from self-assembled polymer droplets. *Sci Rep* 2013; **3**: 1362.
22   Saito M, Koyama K. Deformable microdroplet cavity fabricated by an inkjet method. *Jpn J Appl Phys* 2010; **49**: 092501.
23   Wang CT, Tseng CW, Yu JH, Li YC, Lee CH *et al.* Optical bistability in a silicon nitride microring resonator with azodye-doped liquid crystal as cladding material. *Opt Express* 2013; **21**: 10989–10994.
24   Humar M, Ravnik M, Pajk S, Muševič I. Electrically tunable liquid crystal optical microresonators. *Nat Photonics* 2009; **3**: 595–600.
25   Piegdon KA, Declair S, Förstner J, Meier T, Matthias H *et al.* Tuning quantum-dot based photonic devices with liquid crystals. *Opt Express* 2010; **18**: 7946–7954.
26   Prieto JB, Arbeloa FL, Martinez VM, López TA, Arbeloa IL. photophysical Properties of the pyrromethene 597 dye: solvent effect. *J Phys Chem A* 2004; **108**: 5503–5508.
27   Kondo M, Yu Y, Ikeda T. How does the initial alignment of mesogens affect the photoinduced bending behavior of liquid-crystalline elastomers? *Angew Chem* 2006; **118**: 1406–1410.
28   Ikeda T, Mamiya J, Yu Y. Photomechanics of liquid-crystalline elastomers and other polymers. *Angew Chem Int Ed* 2007; **46**: 506–528.
29   Zeng H, Martella D, Wasylczyk P, Cerretti G, Lavocat JC *et al.* High-resolution 3D direct laser writing for liquid-crystalline elastomer microstructures. *Adv Mater* 2014; **26**: 2319–2322.

Supplementary information for this article can be found on the *Light: Science & Applications*' website (http://www.nature.com/lsa/).